

New insights into atmospherically relevant reaction systems using direct analysis  
in real time-mass spectrometry (DART-MS)

Yue Zhao, Michelle C. Fairhurst, Lisa M. Wingen, Véronique Perraud, Michael J. Ezell, and  
Barbara J. Finlayson-Pitts\*

Department of Chemistry  
University of California  
Irvine, CA 92697, USA

Revision for  
*Atmospheric Measurement Techniques*  
February 21, 2017

\*Corresponding author: Email: [bjfinlay@uci.edu](mailto:bjfinlay@uci.edu); phone: (949) 824-7670; Fax: (949) 824-2420

1 **Abstract**

2 The application of direct analysis in real time mass spectrometry (DART-MS), which is finding  
3 increasing use in atmospheric chemistry, to two different laboratory model systems for airborne  
4 particles is investigated: (1) submicron C<sub>3</sub>-C<sub>7</sub> dicarboxylic acid (diacid) particles reacted with  
5 gas phase trimethylamine (TMA) or butylamine (BA); (2) secondary organic aerosol (SOA)  
6 particles from the ozonolysis of  $\alpha$ -cedrene. The diacid particles exhibit a clear odd-even pattern  
7 in their chemical reactivity toward TMA and BA, with the odd-carbon diacid particles being  
8 substantially more reactive than even ones. The ratio of base to acids in reacted particles,  
9 determined using known acid-base mixtures, was compared to that measured by high resolution  
10 time-of-flight aerosol mass spectrometry (HR-ToF-AMS), which vaporizes the whole particle.  
11 Results show that DART-MS probes ~30 nm of the surface layer, consistent with other studies on  
12 different systems. For  $\alpha$ -cedrene SOA particles, it is shown that varying the temperature of the  
13 particle stream as it enters the DART-MS ionization region can distinguish between specific  
14 components with the same molecular mass but different vapor pressures. These results  
15 demonstrate the utility of DART-MS for (1) examining reactivity of heterogeneous model  
16 systems for atmospheric particles and (2) probing components of SOA particles based on  
17 volatility.

18

19

20

21

## 22 **1. Introduction**

23 Organic aerosol (OA) particles are responsible for ~ 20-90% of atmospheric submicron  
24 particulate matter, with a substantial fraction being secondary organic aerosol (SOA) formed via  
25 oxidation of volatile organic compounds (VOCs) (Zhang et al., 2007;Jimenez et al.,  
26 2009;Hallquist et al., 2009;Ng et al., 2010;Finlayson-Pitts and Pitts, 2000). As a result, the  
27 chemistry and physics of OA particles have been of great interest to the atmospheric science  
28 community over decades. Despite significant progress, many physicochemical processes of OA  
29 particles such as formation, growth, aging, and water uptake remain to be quantitatively  
30 understood which is essential for a better understanding of their impacts on air quality, human  
31 health, visibility and climate (Kroll and Seinfeld, 2008;Hallquist et al., 2009;Laskin et al.,  
32 2015;Ziemann and Atkinson, 2012;Noziere et al., 2015;Glasius and Goldstein, 2016;George et  
33 al., 2015;Moise et al., 2015;Farmer et al., 2015). Atmospheric OA particles consist of hundreds  
34 to thousands of organic compounds with a wide range of functionality, solubility, polarity, and  
35 volatility, and hence pose many challenges and difficulties for characterization of their molecular  
36 composition (Hallquist et al., 2009;Noziere et al., 2015;Glasius and Goldstein, 2016). Therefore,  
37 there is a critical need for implementation of analytical instrumentation which can be applied to  
38 elucidating the composition of OA particles.

39 Recent advances in the development and application of mass spectrometry (MS) techniques for  
40 the analysis of OA particles have been documented in a number of reviews (Noziere et al.,  
41 2015;Laskin et al., 2012;Laskin et al., 2013;Nizkorodov et al., 2011;Pratt and Prather, 2012a, b).  
42 Online particle MS techniques that use relatively high energy vaporization and ionization  
43 processes, e.g., flash vaporization of particles followed by electron ionization (EI) (DeCarlo et al.,  
44 2006;Tobias et al., 2000;Smith et al., 2004) or laser ablation and ionization (Gard et al.,  
45 1997;Zelenyuk and Imre, 2005;Murphy and Thomson, 1995), have advantages of high time  
46 resolution and real-time quantitative information on composition (DeCarlo et al., 2006;Zhang et  
47 al., 2007;Jimenez et al., 2009;Ng et al., 2010;Murphy and Thomson, 1995;Tobias et al.,  
48 2000;Zelenyuk and Imre, 2005;Gard et al., 1997;Pratt and Prather, 2012a, b). However, these  
49 techniques typically cause extensive fragmentation of molecules, providing elemental  
50 information but limited molecular information on individual organic components.

51 In contrast, a number of soft-ionization techniques such as electrospray ionization (ESI),

52 chemical ionization, and photoionization have been deployed to probe the molecular composition  
53 of atmospheric OA particles (Laskin et al., 2012;Laskin et al., 2013;Nizkorodov et al., 2011;Pratt  
54 and Prather, 2012a, b). Variants of ESI such as extractive electrospray ionization mass  
55 spectrometry (EESI-MS) (Chen et al., 2006), have recently been applied to the real-time  
56 measurement of the molecular composition of OA particles (Doezema et al., 2012;Gallimore and  
57 Kalberer, 2013;Horan et al., 2012). In this technique, analyte ionization occurs when the charged  
58 solvent spray intersects the sample stream in front of the MS inlet. However, the mechanism for  
59 the interaction between charged solvent droplets and samples is not yet well understood (Law et  
60 al., 2010;Gallimore and Kalberer, 2013;Jackson et al., 2008;Chen et al., 2006;Chingin et al.,  
61 2008;Wang et al., 2012;Chen et al., 2007). In addition, the use of charged solvent sprays may  
62 lead to in-source ion clustering of analytes, which is prone to occur in ESI-MS (Gao et al.,  
63 2010;Muller et al., 2009b). Chemical ionization mass spectrometry (CIMS) has the advantages  
64 of high sensitivity and selectivity, high time resolution, and has been applied to online detection  
65 of a variety of inorganic and organic gases (Huey, 2007;Noziere et al., 2015). Recently, CIMS  
66 employing thermal desorption techniques has been used to measure the molecular composition of  
67 OA particles collected onto a substrate (Smith et al., 2004;Winkler et al., 2012;Bzdek et al.,  
68 2014;Yatavelli et al., 2012;Lopez-Hilfiker et al., 2014;Aljawhary et al., 2013). As the CIMS  
69 technique with a specific reagent ion is highly selective toward certain classes of organic  
70 compounds, a comprehensive analysis of the molecular composition of OA particles may require  
71 the use of multiple reagent ions. In addition, CIMS is also possibly subject to artifacts from gas  
72 phase ion-clustering (Aljawhary et al., 2013).

73 Direct analysis in real-time mass spectrometry (DART-MS) is an atmospheric pressure soft  
74 ionization technique allowing for real-time *in situ* characterization of the molecular composition  
75 of gaseous, liquid, and solid samples with a wide range of polarities (Cody et al., 2005;Gross,  
76 2014). The samples are directly introduced into the ionization region between the DART ion  
77 source and the MS inlet, where a heated helium gas flow containing metastable helium atoms  
78 ( $\text{He}^*$ ) generated by a corona discharge is used to thermally volatilize and ionize the sample.  
79 Under ambient laboratory conditions, ionization of the analyte occurs primarily through a series  
80 of reactions with secondary species such as protonated water clusters, molecular oxygen ions  
81 ( $\text{O}_2^+$ ), and superoxide anions ( $\text{O}_2^-$ ), generated by the reactions between  $\text{He}^*$  species and  
82 atmospheric water and oxygen molecules. The result is the production of mainly  $[\text{M}+\text{H}]^+$ ,  $\text{M}^+$ ,

83 and  $[M-H]^+$  ions in the positive ion mode, and  $[M-H]^-$  and  $M^-$  ions in the negative ion mode  
84 (Cody et al., 2005;Nah et al., 2013;Gross, 2014).

85 DART-MS has been widely applied to explosive detection, forensic analysis, food analysis, and  
86 clinical and pharmaceutical studies (see the review by Gross (2014) and references therein) as  
87 well as to the analysis of OA particles (Chan et al., 2013;Nah et al., 2013;Chan et al.,  
88 2014;Davies and Wilson, 2015;Zhou et al., 2015;Schilling Fahnestock et al., 2015;Zhao et al.,  
89 2016). For example, Wilson and coworkers demonstrated that DART-MS probes several  
90 nanometers of the surface layer (Nah et al., 2013;Chan et al., 2013) and applied this technique to  
91 investigate the bulk and interface regions of particles during reaction (Nah et al., 2013;Chan et  
92 al., 2013;Chan et al., 2014;Davies and Wilson, 2015). Zhou et al. (Zhou et al., 2015) employed  
93 DART-MS to study the heterogeneous reactions of  $O_3$  with polycyclic aromatic hydrocarbon  
94 films coated on the tip of a glass melting point capillary tube. Schilling Fahnestock et al.  
95 (Schilling Fahnestock et al., 2015) recently reported the first application of DART-MS for off-  
96 line analysis of the composition of SOA from photooxidation of  $C_{12}$  alkanes. In a limited  
97 comparison of DART-MS to ESI-MS, Zhao et al. (Zhao et al., 2016) reported that spectra of  
98 particles from  $\alpha$ -cedrene ozonolysis were similar using the two techniques.

99 In this study, we explore the online application of DART-MS to particles from the reaction of  
100 submicron dicarboxylic acid (diacid) particles with gas phase trimethylamine (TMA) or  
101 butylamine (BA) and also report more detailed studies on SOA particles from ozonolysis of the  
102 sesquiterpene  $\alpha$ -cedrene ( $C_{15}H_{24}$ ). For comparison, measurements by high resolution time-of-  
103 flight aerosol mass spectrometry (HR-ToF-AMS) were also carried out on selected amine-acid  
104 reacted particles. Diacids are among the most abundant components of atmospheric particles,  
105 with a dominant source from photochemical and aqueous phase oxidation processes (Kawamura  
106 and Bikkina, 2016;Ervens et al., 2011;Herrmann et al., 2015). Amines, which are ubiquitous in  
107 air (Ge et al., 2011), play an important role in particle nucleation and growth (Zhang et al.,  
108 2012;Kulmala et al., 2014;Dawson et al., 2012;Chen et al., 2016), formation of light-absorbing  
109 OA particles (Laskin et al., 2015;De Haan et al., 2011;Powelson et al., 2014;Duporte et al., 2016),  
110 as well as aging of OA particles (Laskin et al., 2015;Muller et al., 2009a). Results from this  
111 study provide additional support for the application of DART-MS to probe heterogeneous  
112 atmospheric reactions, and to provide additional insights into the nature of organic constituents  
113 in complex SOA particles.

## 114 2. Experimental

### 115 2.1 Generation and reaction of diacid particles with gas phase amines

116 Figure 1 is a schematic diagram of the glass flow reactor (Zhao et al., 2015) used to investigate  
117 reactions between gas phase amines (trimethylamine or butylamine) and particles of malonic  
118 acid (C<sub>3</sub>), succinic acid (C<sub>4</sub>), glutaric acid (C<sub>5</sub>), adipic acid (C<sub>6</sub>), and pimelic acid (C<sub>7</sub>). Gas  
119 phase trimethylamine (TMA) was generated by passing 1.0 L min<sup>-1</sup> of clean dry air (Praxair, ultra  
120 zero air) through a U-shaped glass holder containing pure liquid TMA sealed inside a permeation  
121 tube (VICI Metronics Inc). Generation of gas phase butylamine (BA) was achieved by injecting  
122 an aqueous solution (1% v/v), prepared from pure liquid BA (Sigma-Aldrich, 99.5%) and  
123 nanopure water (18.2 MΩ cm), into a flow of 0.5 L min<sup>-1</sup> of dry air using an automated syringe  
124 pump (Pump Systems Inc., model NE-1000) at a rate of 2.4 μL hr<sup>-1</sup>. The concentration of TMA  
125 in the air flow exiting the permeation tube was measured by collection onto a weak cation  
126 exchange resin followed by extraction and analysis using ion chromatography as described  
127 previously (Dawson et al., 2014). The initial concentration of TMA in the flow reactor was  
128 calculated to be 50 ppb based on the measured concentration from the permeation tube and the  
129 dilution factor. The initial concentration of BA, calculated from the amount of the aqueous  
130 solution injected and the total air flow in the reactor, was also 50 ppb.

131 For each experiment, the flow reactor was first conditioned overnight with either 1.0 L min<sup>-1</sup>  
132 TMA or 0.5 L min<sup>-1</sup> BA in addition to clean, dry air so that the total flow was ~ 2 L min<sup>-1</sup>. When  
133 the gas phase concentration of the amine became stable as indicated by DART-MS signals, a  
134 small flow (0.2-0.5 L min<sup>-1</sup>) of air containing dry diacid particles was added to the flow reactor  
135 upstream of the amine inlet. The flow of clean, dry air was adjusted to bring the total flow in the  
136 reactor to 2.0 L min<sup>-1</sup> corresponding to a residence time of 44 s. Acid particles were generated by  
137 atomizing aqueous solutions of the corresponding diacid (1 g L<sup>-1</sup> in nanopure water) using an  
138 atomizer (TSI, model 3076) and dried by passing through two diffusion dryers in series (TSI,  
139 model 3062). The desiccant inside the dryers was replaced daily to minimize water associated  
140 with the particles. The relative humidity (RH) in the flow reactor was < 5% as measured by a  
141 humidity probe (Vaisala, HMT234). All diacids were purchased from Sigma-Aldrich and have a  
142 stated purity of > 99 %. The size distribution of the particles formed in the flow reactor was  
143 measured using a scanning mobility particle sizer (SMPS, TSI) consisting of an electrostatic

144 classifier (model 3080), a long differential mobility analyzer (model 3081), and a condensation  
145 particle counter (model 3025A or 3776). The SMPS was operated with a sheath flow of 3 LPM  
146 and an aerosol flow of 0.3 LPM. Because the flow system required extensive conditioning with  
147 the amine prior to introducing the diacid particles, the size distributions represent particles after  
148 reaction with amines. Typical surface weighted size distributions are shown in Fig. S1, and the  
149 different weighted geometric mean diameters ( $\bar{D}_{g,x}$ , where  $x$  = number (N), surface (S), or volume  
150 (V)) and the total concentrations for all diacid particles are given in Table S1.

151 The amine-reacted particle stream (PS) exiting the flow reactor was either directly introduced  
152 into the DART ionization region for online measurement of the total (gas phase + particle-bound)  
153 amines, or passed through a 10 cm monolith carbon denuder (Novacarb<sup>TM</sup>; Mast Carbon, Ltd.) to  
154 remove gases and measure only particle-bound amines and diacids. The denuder was maintained  
155 at room temperature ( $T_{PS} = 23$  °C). As discussed below, the fraction of particle-bound amines  
156 was corrected for particle loss in the denuder, which was ~ 10 % at room temperature (Fig. S1).

## 157 **2.2 $\alpha$ -Cedrene SOA particles generation**

158 Ozonolysis of  $\alpha$ -cedrene in the absence of seed particles or OH scavengers was used to generate  
159 SOA particles under dry conditions in the glass flow reactor described previously (Zhao et al.,  
160 2016). Gas phase  $\alpha$ -cedrene was generated by injecting the pure liquid (Sigma-Aldrich, > 98%)  
161 into a flow (1.8 or 3.0 L min<sup>-1</sup>) of clean, dry air using an automated syringe pump. Ozone,  
162 produced by passing a flow of 0.24 L min<sup>-1</sup> of O<sub>2</sub> (Praxair, Ultra High Purity, 99.993%) through a  
163 Pen-Ray mercury lamp (model 11SC-2) was added to the flow reactor downstream of the  $\alpha$ -  
164 cedrene inlet. The total gas flow in the reactor was 2.0 or 3.2 L min<sup>-1</sup>, giving a residence time of  
165 44 or 27 s, respectively. The initial  $\alpha$ -cedrene concentration, calculated from the amount of  $\alpha$ -  
166 cedrene liquid injected into the reactor and the total gas flow, was 138 ppb. The initial O<sub>3</sub>  
167 concentration, measured at the source using a UV-VIS spectrometer (Ocean Optics, HR4000),  
168 was calculated to be 16 ppm in the reactor after dilution.

169 Size distributions of SOA particles formed in the flow reactor at the two residence times (44 or  
170 27 s) were also measured using SMPS (sheath and aerosol flows were 15 LPM and 1.5 LPM,  
171 respectively). Typical surface weighted geometric mean diameters ( $\bar{D}_{g,S}$ ) were measured to be 28  
172 nm and 21 nm, and number weighted diameters were ( $\bar{D}_{g,N}$ ) of 24 and 16 nm, respectively. Once

173 stable, the chemical composition of these particles at both reaction times was measured online  
174 using DART-MS. Before entering into the DART ionization region,  $2.0 \text{ L min}^{-1}$  of particle  
175 stream (PS) exiting the reactor was first passed through a 10 cm monolith carbon denuder to  
176 remove the gas phase species and then heated to different temperatures (up to  $T_{\text{PS}} = 160 \text{ }^\circ\text{C}$ ) in a  
177 stainless steel tube wrapped with a heating tape. The residence time of the particle stream in the  
178 heated tube was  $\sim 4 \text{ s}$ . Although the use of the denuder caused a  $\sim 30\%$  loss of SOA particles at  
179 room temperature, it has no significant influence on the size distribution for which a typical  
180 example is shown in Fig. S2.

### 181 **2.3 DART-MS measurements operating conditions**

182 The chemical composition of either amine-reacted diacid particles or  $\alpha$ -cedrene SOA particles  
183 was measured online using a Xevo TQS triple quadrupole mass spectrometer (Waters) equipped  
184 with a commercial DART ion source (IonSense, DART SVP with Vapur<sup>®</sup> Interface). The DART  
185 probe was placed at the entrance of the MS, with a distance of 5 mm and a relative angle of  $180^\circ$   
186 (Fig. 1), and was operated under the following conditions: He reagent gas flow  $3.1 \text{ L min}^{-1}$ ; He  
187 gas temperature  $350 \text{ }^\circ\text{C}$  (which gives a measured temperature of  $\sim 260 \text{ }^\circ\text{C}$  in the ionization region  
188 with or without particle stream flow (Fig. S3)); grid electrode voltage 350 V. Mass spectra were  
189 collected in the range  $m/z$  20-500 for the amine-diacid particle system and  $m/z$  100-1000 for  $\alpha$ -  
190 cedrene SOA particles. Each spectrum was acquired by averaging the signal over 2-4 min of  
191 sampling time. Background spectra were also recorded by measuring a clean air stream under  
192 conditions identical to those for online particle stream measurements and subtracted from  
193 particle spectra.

### 194 **2.4 DART-MS analysis of amine-reacted diacid particles**

195 For the amine-diacid particle system, both the gas phase and particle-bound amines were  
196 detected as  $[\text{M}+\text{H}]^+$  ions in the positive ion mode, and the diacids as  $[\text{M}-\text{H}]^-$  in the negative ion  
197 mode. Diacid-amine clusters were not observed in the mass spectra (Fig. S4). As described  
198 earlier, the particle-bound and the total (gas phase + particle-bound) amines can be measured in  
199 the presence and absence of a denuder, respectively. Thus, assuming the same ionization  
200 efficiency for the gas-phase and particle-phase amines, the fraction of amine taken up by the  
201 particles ( $f_p$ ) can be derived from Eq. (1),



$$f_p = \frac{\text{amine ion signal measured with denuder} \times C_f}{\text{amine ion signal measured without denuder}} \quad (1)$$

202 where  $C_f$  is the correction factor for the particle loss in the denuder and has a value of 1.1 (SI  
 203 section 1). The value of  $f_p$  can be an indicator of the reactivity of diacid particles toward amines.  
 204 Given the difference in surface area concentrations of different diacid particles (Table S1), the  
 205 measured  $f_p$  was normalized to an arbitrary reference surface area of  $1 \times 10^{-4} \text{ cm}^2 \text{ cm}^{-3}$  for direct  
 206 comparisons of the reactivity of different amine-diacid systems. Thus, the particle-phase fraction  
 207 of amine taken up by the diacid normalized by surface area, ( $F_p$ ) is given by:

$$F_p = \frac{f_p}{\frac{\text{aerosol surface area concentration (cm}^2 \text{ cm}^{-3})}{\text{reference surface area (cm}^2 \text{ cm}^{-3})}} \quad (2)$$

208 The molar ratio ( $R_{B/A}$ ) of amine (base, B) to diacid (A) in amine-reacted diacid particles can also  
 209 provide important insights into the reactivity of the diacid particles toward amines. Values of  
 210  $R_{B/A}$  were derived first from four aqueous standard solutions with different amine concentrations  
 211 (0.5-10 mM) but constant diacid concentrations (10 mM) for each amine-diacid system. As  
 212 shown below, this covers the range measured for the reacted particles. A melting point capillary  
 213 tube was dipped into the standard solution and immediately placed into the DART ionization  
 214 region for analysis. A linear relationship between the base-to-acid molar ratio ( $R_{B/A}$ ) of the  
 215 aqueous solutions and the corresponding DART-MS signal ratios for amine ( $[\text{M}+\text{H}]^+$ ) to acid  
 216 ( $[\text{M}-\text{H}]^-$ ) was observed for each standard solution (Fig. S5). These relationships were then used  
 217 to estimate the  $R_{B/A}$  value in amine-reacted diacid particles.

## 218 **2.5 DART-MS analysis of $\alpha$ -cedrene SOA particles**

219  $\alpha$ -Cedrene SOA particles were analyzed in the negative ion mode, where the deprotonated  $[\text{M}-$   
 220  $\text{H}]^-$  ions dominate. In other studies, DART-MS was proposed to preferentially probe the surface  
 221 layers of particles and the measured ion signal was sensitive to the volatility of the analytes (Nah  
 222 et al., 2013; Chan et al., 2013). In the present studies, the gas phase species were removed by a  
 223 denuder and the particle stream was then exposed to temperatures up to  $160^\circ\text{C}$  prior to  
 224 introduction into the DART ionization region in order to probe the bulk of the particles and low  
 225 volatility components of SOA particles such as HMW products.

## 226 **2.6 HR-TOF-AMS measurements**

227 In some experiments, the chemical composition of TMA-reacted diacid particles was also  
228 analyzed online using an Aerodyne high resolution aerosol mass spectrometer (HR-ToF-AMS).  
229 Analysis of HR-ToF-AMS high resolution mass spectra was carried out using SQUIRREL  
230 V1.56D-1.57I and PIKA V1.15D-1.61I analysis software with IGOR Pro (Wavemetrics, Inc.).  
231 Default values for the fragmentation tables were used except for corrections to the isotopic  
232 abundance of  $^{15}\text{N}^{14}\text{N}$  which is not resolved from  $\text{CHO}^+$  at  $m/z$  29 and was quantified for each  
233 experiment with the use of a particle filter (Canagaratna et al., 2015). Default relative ionization  
234 efficiencies (RIE) values were used for all organics, while that for TMA was measured as  
235 discussed in the SI (section 5). TMA-reacted diacid particles with and without a denuder gave  
236 similar results and were averaged to generate mass spectra for each TMA-diacid system (Fig. S6).  
237 From these mass spectra, the ratio of  $\text{C}_x\text{H}_y\text{N}_1^+$  fragments to the sum of  $\text{C}_x\text{H}_y^+$  and  $\text{C}_x\text{H}_y\text{O}_z^+$   
238 fragments, which is a measure of the ratio of amine to diacid, was determined for each TMA-  
239 diacid system (Fig. S7). Because these particles are efficiently vaporized at the vaporizer  
240 temperature employed ( $T_{\text{vap}} = 600^\circ$ ), the amine to diacid ratios from HR-ToF-AMS  
241 measurements reflect the overall composition of the particle ensemble.

## 242 **3. Results and Discussion**

### 243 **3.1 Reaction of diacid particles with gas phase amines**

#### 244 **3.1.1 DART-MS data**

245 Figure 2 shows the surface area normalized fraction ( $F_p$ ) of BA or TMA in the particle phase of  
246 amine-reacted  $\text{C}_3$ - $\text{C}_7$  diacid particles as a function of carbon number. The odd-carbon diacids  
247 take up much more base than the even-carbon acids, with no particle-bound amines detected for  
248 the  $\text{C}_4$  and  $\text{C}_6$  acids. The measured  $F_p$  values for both amines decrease with increasing carbon  
249 number, with no particle bound TMA observed for pimelic acid ( $\text{C}_7$ ). An odd-even alternation in  
250 physical properties such as melting point (Thalladi et al., 2000), vapor pressure (Bilde et al.,  
251 2003;Bilde et al., 2015;Cappa et al., 2007;Bruns et al., 2012), and solubility (Zhang et al., 2013)  
252 is well known for diacids. While some studies have probed a possible odd-even alternation in  
253 their reactivity with  $\text{HO}_2$  (Taketani et al., 2013),  $\text{NO}_3$  (de Semainville et al., 2010), and  $\text{N}_2\text{O}_5$   
254 (Griffiths et al., 2009), as well as in their  $\text{TiO}_2$ -based photocatalytic degradation (Sun et al.,

255 2014), extensive investigations of differences in chemical reactivity between odd and even  
256 diacids with amines have not been carried out.

257 The alternating behaviors between odd and even diacids have generally been attributed to the  
258 differences in their crystal structures. For example, odd-carbon diacids have higher aqueous  
259 solubility than even-carbon diacids because of the energetically unfavorable and looser crystal  
260 packing for the former, which facilitates penetration of water molecules between the molecular  
261 planes to dissolve the crystal (Zhang et al., 2013). It is possible that small amines, like water  
262 molecules, can also disrupt the crystal lattice of odd-carbon diacids more readily than that of the  
263 even-carbon species, thus leading to the observed odd-even alternation in the chemical reactivity.  
264 This may also explain why uptake of TMA is significantly smaller than BA (Fig. 2), where the  
265 bulky TMA structure may hinder the penetration and disruption of the acid crystal lattice. A  
266 similar steric effect has also been reported by Liu et al. (Liu et al., 2012) to explain the trends in  
267 reactivity on citric acid and humic acid particles of methylamine, dimethylamine, and TMA,  
268 which decreases with an increasing number of methyl groups.

269 Alternatively, the odd-even differences could be due to differences in surface composition and  
270 structure. Ruehl and Wilson (Ruehl and Wilson, 2014) observed an odd-even alternation in the  
271 hygroscopic growth of aqueous ammonium sulfate particles with a diacid shell. They attributed  
272 this behavior to the differences in the surface orientation of odd and even diacids on aqueous  
273 droplets, i.e., the “end to end” alignment with only one carboxyl group in contact with the  
274 aqueous phase for odd-carbon diacids versus the “folded” arrangement with both carboxyl  
275 groups in contact with the aqueous phase for the even-carbon acids. If a similar effect is present  
276 in the solids, an odd-even alternation in the reactivity with amines could result due to differences  
277 in surface availability of the  $\text{-COOH}$  groups.

278 Based on previous work by Lavi et al. (Lavi et al., 2015) the diacid and their alkylammonium salts  
279 vaporize well below  $100\text{ }^{\circ}\text{C}$ . Thus, in some experiments, the amine-reacted diacid particles  
280 were heated after exiting the 10-cm monolith denuder and prior to entering the DART-MS  
281 ionization region to probe whether the amine was distributed throughout the bulk of the particle  
282 or segregated on the surface. As seen in Fig. 3, there is no obvious temperature dependence,  
283 indicating that all of the amines in the particles are being sampled under all conditions. One  
284 explanation is that the entire particle is being sampled. Alternatively, if the amine reactions are

285 restricted to a surface layer as is common for gas-solid interactions, then the surface layer being  
286 probed at all  $T_{PS}$  is sufficiently deep to detect the entire particle-bound base. We show in the  
287 following that the latter is the likely explanation.

288 The molar ratio of amine to diacid ( $R_{B/A}$ ) in amine-reacted diacid particles was estimated by  
289 comparing the DART-MS signal intensity ratio of amine to diacid measured at  $T_{PS} = 23$  °C with  
290 that for known amine-diacid standard solutions (Fig. S5). As listed in Table 1, the  $R_{B/A}$  values  
291 follow a similar trend as  $F_p$  (Fig. 2) for TMA- and BA-reacted malonic acid ( $C_3$ ) and glutaric  
292 acid ( $C_5$ ) particles.

293 However, the value of  $R_{B/A}$  for BA-reacted pimelic acid ( $C_7$ ) particles is larger than that for BA-  
294 reacted glutaric acid and malonic acid, inconsistent with the trend in  $F_p$ . A possible explanation  
295 can be suggested based on differences in the relative saturation vapor pressures ( $P_{sat}$ ) (Bilde et al.,  
296 2015) of these diacids. It has been shown that the probe depth of online DART-MS is positively  
297 correlated with the volatility of straight chain even-diacid particles (Chan et al., 2013). Given  
298 that the volatility of  $C_7$  ( $P_{sat} = 1.1 \times 10^{-10}$  atm) is substantially lower than that of both  $C_3$  and  $C_5$   
299 which are  $\sim 1.7 \times 10^{-9}$  atm, the probe depth for  $C_7$  particles is expected to be significantly smaller  
300 than the other two diacid particles, i.e., about a factor of 8 if the probe depth-volatility  
301 relationship reported for the even-diacid particles is extrapolated to the odd-diacids (Fig. S8).  
302 Correcting for this, the  $R_{B/A}$  value would be about a factor of 8 smaller, i.e.,  $\sim 0.05$ , which would  
303 follow the trend for the  $F_p$  values for all three amine-reacted odd-diacid particles. Note that  
304 although the probe depth may be smaller for  $C_7$ , the  $F_p$  value (Fig. 2) for the BA reaction  
305 suggests that it is still sufficient to detect all of the particle-bound amine (Fig. 3).

### 306 **3.1.2 Comparison with HR-ToF-AMS data**

307 The  $R_{B/A}$  values for TMA-reacted  $C_3$  and  $C_5$  diacid particles were also measured using HR-ToF-  
308 AMS and are shown in Table 1 and Fig. S7. The  $R_{B/A}$  values for malonic acid and glutaric acid  
309 particles measured by HR-ToF-AMS are smaller than the corresponding values determined by  
310 DART-MS. The interaction between amines and carboxylic acids forms aminium carboxylate  
311 salts (Liu et al., 2012; Angelino et al., 2001; Lavi et al., 2015; Gomez-Hernandez et al., 2016), so  
312 that the gas-solid reaction is expected to form a surface layer of the salt. However, HR-ToF-  
313 AMS measures the entire particle (i.e., both the surface reacted layer and the unreacted bulk).

314 The larger  $R_{B/A}$  values from DART-MS show that it is probing the reacted surface layer  
 315 containing the aminium salt, plus perhaps some fraction of the underlying diacid. This is  
 316 consistent with other studies where DART-MS was shown to probe mainly the surface layer  
 317 (Chan et al., 2013; Nah et al., 2013).

318 In addition to direct measurements by HR-ToF-AMS, the  $R_{B/A}$  values for the entire amine-reacted  
 319 diacid particles can also be estimated by combining DART-MS with SMPS data. The number of  
 320 amine molecules in the particles per  $\text{cm}^3$  air ( $N_{p\text{-amine}}$ , molecules  $\text{cm}^{-3}$  air, Table S2) can be  
 321 derived from Eq. (3),

$$N_{p\text{-amine}} = F_p \times N_{total} \quad (3)$$

322 where  $F_p$  is as defined in Eq. (2) above and  $N_{total}$  is the amount of amines in the gas phase plus  
 323 those bound to the particles (molecules  $\text{cm}^{-3}$ ) estimated from the DART-MS signal for the total  
 324 amines and the DART-MS sensitivity to amines calibrated using gas phase amines with known  
 325 concentrations generated as described in the experimental section. The number of diacid  
 326 molecules in the particles per  $\text{cm}^3$  air ( $N_{p\text{-acid}}$ ) can be estimated from Eq. (4),

$$N_{p\text{-acid}} = \frac{[(V_p \times \rho) - m_{p\text{-amine}}] \times N_A}{MW_{acid}} \quad (4)$$

327 where  $V_p$  is the total volume concentration of amine-reacted diacid particles measured by SMPS  
 328 ( $\text{cm}^3$  particle volume per  $\text{cm}^{-3}$  air);  $\rho$  is the density of amine-reacted diacid particles, which is  
 329 assumed to be the same as the solid diacid samples (i.e., 1.619  $\text{g cm}^{-3}$  for malonic acid, 1.429  $\text{g}$   
 330  $\text{cm}^{-3}$  for glutaric acid, and 1.329  $\text{g cm}^{-3}$  for pimelic acid (Lide, 2004));  $m_{p\text{-amine}}$  is the mass  
 331 concentration of particle phase amines ( $\text{g cm}^{-3}$  air), which can be determined from Eq. (3);  
 332  $MW_{acid}$  is the molecular weight of the corresponding diacid ( $\text{g mol}^{-1}$ ); and  $N_A$  is Avogadro's  
 333 number.

334 The  $R_{B/A}$  values calculated from the ratio of  $N_{p\text{-amine}}$  to  $N_{p\text{-acid}}$  are presented in Table 1. They are  
 335 significantly smaller than those directly determined by DART-MS, further confirming that  
 336 DART-MS mainly probes the surface layer of particles, and that the amines are segregated at the  
 337 surface.

338 However, the calculated values are also smaller than the values measured by HR-ToF-AMS.

339 This is likely because the densities of the pure diacids were used in the calculations. Salts  
 340 formed by reaction of amines with diacids tend to have densities that are smaller by as much as  
 341 ~30% (Lavi et al., 2015). Small decreases in particle density would decrease the calculated  
 342 particle mass concentrations and  $N_{p-acid}$  (Eq. (4)), and hence increase calculated  $R_{B/A}$  values.  
 343 Despite the difference in the absolute values of  $R_{B/A}$ , the trends in  $R_{B/A}$  values for TMA-reacted  
 344 malonic acid and glutaric acid particles derived by DART-MS, HR-ToF-AMS, and calculations  
 345 are consistent within the experimental uncertainty.

### 346 3.1.3 Estimation of probe depth for TMA-reacted odd diacid particles

347 When an amine reacts with a diacid, the resulting particle with radius  $R$ , is assumed to contain a  
 348 diacid core ( $r_1$ ), and an aminium salt shell of thickness  $L_{shell} = (R - r_1)$  as shown in Fig. 4. The  
 349 total volume of the particle, assuming a spherical geometry, can be expressed as:

$$350 \quad V_{total} = \frac{4}{3}\pi R^3 \quad (5)$$

351  $V_{total}$  can be obtained directly from SMPS data (Table S1). Since the total particle is comprised  
 352 of the acid core and aminium salt shell, the total volume can also be expressed as,

$$353 \quad V_{total} = V_s + V_c \quad (6)$$

354 where  $V_c$  is the volume of the acid core and  $V_s$  is the volume of the aminium salt shell. The  
 355 volume of the shell can be obtained from the experimental data as follows:

$$356 \quad V_s = \frac{m_s}{\rho_s} = \frac{n_s MW_s}{\rho_s} \quad (7)$$

357 In Eq. (7),  $m_s$  is the mass of the aminium salt,  $\rho_s$  is the density of the salt,  $n_s$  is the number of  
 358 moles of salt per  $\text{cm}^3$  air, and  $MW_s$  is the molecular weight of the aminium salt. Note that two  
 359 values of  $V_s$  can be calculated if aminium salt forms with stoichiometric molar amine:acid ratios  
 360 of either 1:1 or 2:1. In addition, the densities of the aminium salts are reported to be less than  
 361 that of the pure acid, as much as ~30% lower for the 2:1 salt (Lavi et al., 2015). For the  
 362 calculations below, the density of the salt is taken to be either 15% smaller than the acid for a 1:1  
 363 base-to-acid salt or 30% smaller for the 2:1 salt.

364 Thus, one can solve for  $r_1$  as follows:

$$365 \quad \frac{R}{r_1} = \left( \frac{V_{total}}{V_{core}} \right)^{\frac{1}{3}} = \left( \frac{V_{total}}{V_{total} - V_s} \right)^{\frac{1}{3}} \quad (8)$$

366 Using the volume weighted geometric mean diameter (nm) (Table S1) in Eq. (8) to obtain R, the  
 367 radius of the acid core,  $r_I$ , as well as the thickness of the salt layer,  $L_{shell}$  ( $L_{shell} = R - r_I$ ) can be  
 368 obtained. Table 2 summarizes the results for TMA-reacted malonic acid and glutaric acid  
 369 particles.

370 The probe depth ( $L_{DART}$ ) is assumed to be comprised of the aminium salt shell (shaded red area)  
 371 and some fraction of the acid core (shaded green area) (Fig. 4). The thickness of the aminium  
 372 salt layer determined previously ( $L_{shell}$ ) along with the ratio of  $R_{B/A}$  values for a given diacid  
 373 derived by DART-MS and HR-ToF-AMS (Table 1) can be used to estimate the probe depth of  
 374 the reacted particles in the following manner.

375 As discussed earlier, the independence of  $F_p$  on particle stream temperature ( $T_{ps}$ ) (Fig. 3)  
 376 suggests that DART-MS probes all of the aminium salt shell plus likely *some* of the pure acid  
 377 core. On the other hand, HR-ToF-AMS (by measuring the entire particles) probes the total  
 378 amount of the amine present in the particles and *all* of the pure acid core. Thus, the ratio of the  
 379  $R_{B/A}$  values from DART-MS to that of the HR-ToF-AMS can be expressed as:

$$380 \quad \frac{R_{B/A,DART}}{R_{B/A,AMS}} = \frac{\frac{\text{moles } B(DART)}{\text{moles } A(DART)}}{\frac{\text{moles } B(AMS)}{\text{moles } A(AMS)}} = \frac{\text{moles } A(AMS)}{\text{moles } A(DART)} \quad (9)$$

381 The total volume of a particle can be expressed as a function of the different areas labelled in Fig.  
 382 4 as,

$$383 \quad V_{total} = V_s + V_m + V_{uc} \quad (10)$$

384 where,  $V_s$ ,  $V_m$  and  $V_{uc}$  are the volume of the salt shell (shaded red area), the volume of the middle  
 385 layer (i.e. the volume of the acid core that is probed by DART-MS, shaded green area) and the  
 386 volume of the core that is not probed by DART (yellow area) respectively ( $V_{uc}$  = unprobed core).  
 387 While DART-MS is assumed to probe the salt layer and some fraction of the acid core, the HR-  
 388 ToF-AMS will probe the entire bulk of the particle. As a result, Eq. (9) can be expressed as  
 389 follows,

390

$$\frac{R_{B/A,DART}}{R_{B/A,AMS}} = \frac{\frac{\rho_s V_s}{MW_s} + \frac{\rho_A V_m}{MW_A} + \frac{\rho_A V_{uc}}{MW_A}}{\frac{\rho_s V_s}{MW_s} + \frac{\rho_A V_m}{MW_A}} \quad (11)$$

391 where  $\rho_s$  and  $MW_s$  are the density and molecular weight for the aminium salt,  $\rho_A$  and  $MW_A$  are the  
 392 density and molecular weight of the diacid contained in the ‘middle’ layer and the acid core that  
 393 is not probed by DART-MS.

394 The ratio of the base-to-acid molar ratio from DART-MS to that of the HR-ToF-AMS is  $\sim 2$   
 395 (Table 1). As such, Eq. (11) can be simplified to yield Eq. (12):

396

$$\frac{\rho_s V_s}{MW_s} + \frac{\rho_A V_m}{MW_A} = \frac{\rho_A V_{uc}}{MW_A} \quad (12)$$

397 The spherical volumes of each section of the particle can now be expressed in terms of their  
 398 respective radii based on Fig. 4:

399

$$\frac{\rho_s (R^3 - r_1^3)}{MW_s} + \frac{\rho_A (r_1^3 - r_2^3)}{MW_A} = \frac{\rho_A r_2^3}{MW_A} \quad (13)$$

400 The values of  $r_2$  corresponding to a stoichiometric molar amine:acid ratio of 1:1 or 2:1 can then  
 401 be derived along with the derived probe depth for DART-MS,  $L_{DART} = (R - r_2)$ . As can be seen in  
 402 Table 2, using the volume weighted geometric mean diameter for the TMA-reacted malonic acid  
 403 of 290 nm (Table S1), the decrease in the DART-MS ratio of  $R_{B/A}$  from 0.28 to 0.14 for HR-ToF-  
 404 AMS is consistent with a probe depth of  $\sim 32$  nm, and is similar for glutaric acid,  $\sim 28$  nm. It is  
 405 worth noting that the values obtained for  $r_2$  and  $L_{DART}$  are essentially independent of the assumed  
 406 stoichiometry and would yield the same value for any mixture of 1:1 and 2:1 salt.

### 407 3.2 Characterization of $\alpha$ -cedrene SOA particles

408 In earlier studies (Zhao et al., 2016), limited DART-MS measurements were made for SOA  
 409 particles at  $T_{PS} = 160$  °C from the ozonolysis of  $\alpha$ -cedrene for purposes of confirming high  
 410 molecular weight (HMW) products identified in ESI mass spectra. More extensive  
 411 measurements were carried out here to investigate in more detail the application of DART-MS to  
 412 organic particles of complex composition. Figure 5 shows DART(-) (negative ion mode) mass  
 413 spectra of polydisperse  $\alpha$ -cedrene SOA particles measured as a function of  $T_{PS}$  for distributions



414 with different  $\bar{D}_{g,S}$ , 21 nm and 28 nm. The ion signals observed in the mass spectra of SOA  
415 particles at  $T_{PS} = 23$  °C (Figs. 5a and 5c) are dominated by low molecular weight (LMW)  
416 products ( $m/z$  200-350), with a small contribution from HMW products ( $m/z$  420-580). This is  
417 not surprising given the very short particle residence time in the ionization region (estimated to  
418 be of the order of milliseconds under our conditions), which limits the vaporization of low  
419 volatility HMW products from SOA particles. However, the signal intensities of HMW products  
420 as well as most of the LMW products increase substantially at  $T_{PS} = 125$  °C (Figs. 5b and 5d). It  
421 is not known if the entire particle is vaporized at this temperature, although essentially complete  
422 vaporization has been reported for larger SOA particles precursors (Kolesar et al., 2015). Many  
423 of the LMW products in  $\alpha$ -cedrene SOA particles observed in DART mass spectra were also  
424 detected using GC-MS (Jaoui et al., 2004; Yao et al., 2014; Jaoui et al., 2013) and APCI-MS  
425 (Reinnig et al., 2009) in other studies. The possible structures and formation mechanism of  
426 many of these LMW products were investigated in previous studies (Jaoui et al., 2004; Reinnig et  
427 al., 2009; Jaoui et al., 2013; Yao et al., 2014; Zhao et al., 2016) and those for HMW products in  
428 our previous study (Zhao et al., 2016).

429 Potential artifacts in DART-MS with respect to in-source oxidation chemistry and gas phase ion  
430 clustering of organic compounds that forms non-covalently bound HMW species were evaluated  
431 by analyzing different organic standards and  $\alpha$ -cedrene SOA particles in the negative ion mode  
432 under varying controlled conditions. Details of the analysis and results can be found in Section 8  
433 of the SI. The results show that measurements of diacid particles and  $\alpha$ -cedrene SOA particles  
434 with DART-MS do not suffer from in-source oxidation and gas phase clustering artifacts.

435 Differences in DART mass spectra of  $\alpha$ -cedrene SOA particles at  $T_{PS} = 23$  °C or 125 °C in Fig. 5  
436 are consistent with a dependence of product distribution on particle size as reported earlier based  
437 on ESI-MS (Zhao et al., 2016). To better explore the size- and temperature-dependent product  
438 distribution in  $\alpha$ -cedrene SOA particles, the intensity ratio of HMW to LMW products as well as  
439 the intensity fraction of the two prominent LMW products, i.e.,  $m/z$  253 and  $m/z$  267, was  
440 examined as a function of  $T_{PS}$  and particle size. Figure 6a shows the signal intensity ratio of  
441 HMW products (summed over  $m/z$  420-580) to that of LMW products (summed over  $m/z$  200-  
442 350) for  $\alpha$ -cedrene SOA particles with a  $\bar{D}_{g,S}$  of 21 nm and 28 nm at different  $T_{PS}$ . Smaller  
443 particles at each  $T_{PS}$  show a greater contribution from HMW products to the total ion signal,

444 consistent with these products serving as important agents for initial particle formation (Zhao et  
445 al., 2016).

446 In our previous study (Zhao et al., 2016), HR-ToF-AMS was used to characterize the bulk  
447 composition of  $\alpha$ -cedrene ozonolysis particles generated in Teflon chambers. Under dry  
448 conditions (<5%), chamber-generated particles had an O:C = 0.34, which was characteristic of  
449 LMW products that were shown to contribute primarily to particle growth rather than to initial  
450 particle formation. This is not necessarily surprising since the chamber-generated particles had  
451 undergone significantly more particle growth ( $\bar{D}_{g,N} \sim 70$  nm) than particles generated in the flow  
452 reactor ( $\bar{D}_{g,N} < 30$  nm), which are too small to transmit through the HR-ToF-AMS lens. While  
453 bulk particle composition measurements by AMS were limited to chamber particles, their  
454 comparison to DART-MS measurements show that LMW components make up the majority of  
455 the particle mass at long reaction times. This highlights the value of DART-MS in accessing the  
456 markedly different compositions at varied extent of particle growth.

457 Figure 6b shows the intensity fraction of products with peaks at  $m/z$  253 or  $m/z$  267 to the total  
458 LMW products ( $m/z$  200-350) at different  $T_{PS}$  for polydisperse  $\alpha$ -cedrene SOA particles with  
459 distributions having a  $\bar{D}_{g,S}$  centered at 21 nm and 28 nm, respectively. For both distributions, the  
460 fraction of product  $m/z$  253 increases with rising  $T_{PS}$  whereas that of product  $m/z$  267 decreases  
461 with increasing  $T_{PS}$ . The distinct temperature dependence of these two peaks may indicate that  
462 the product responsible for  $m/z$  253 has a lower volatility than product  $m/z$  267 (although a  
463 contribution from decomposition of HMW products at higher  $T_{PS}$  cannot be ruled out). Smaller  
464 particles tend to have a greater fraction of  $m/z$  253 compared to larger particles but a lower  
465 fraction from  $m/z$  267. This suggests that the species responsible for  $m/z$  253 play a more  
466 important role in the early stages of particle growth, consistent with its lower volatility. Previous  
467 studies have proposed multiple isomeric structures, i.e.,  $\alpha$ -cedrinic acid and 10-hydroxy- $\alpha$ -  
468 norcedralic acid for product  $m/z$  253 (Jaoui et al., 2004;Reinnig et al., 2009;Jaoui et al., 2013;Yao  
469 et al., 2014;Zhao et al., 2016). Using the EVAPORATION model (Compernelle et al., 2011), the  
470  $P_{sat}$  of  $\alpha$ -cedrinic acid and 10-hydroxy- $\alpha$ -norcedralic acid are estimated to be  $2.4 \times 10^{-12}$  atm and  
471  $5.1 \times 10^{-11}$  atm, respectively, and the  $P_{sat}$  of the structures proposed for  $m/z$  267 is estimated to be  
472  $(0.39-3.1) \times 10^{-11}$  atm (Zhao et al., 2016). Therefore,  $\alpha$ -cedrinic acid, the  $P_{sat}$  of which is lower  
473 than all possible isomeric structures of  $m/z$  263, is likely the dominant structure for the product

474  $m/z$  253. This illustrates that DART-MS measurements may help resolve structural isomers of  
475 some products by providing information on their volatility.

#### 476 **4. Conclusions**

477 DART-MS was successfully applied to the real-time study of the reaction of submicron diacid  
478 particles with gas phase amines and to the chemical composition of nanometer-sized SOA  
479 particles from ozonolysis of  $\alpha$ -cedrene. The reactivity of  $C_3$ - $C_7$  diacid particles toward TMA and  
480 BA exhibits a clear alternation between the odd and even carbon numbers. Calibrations using  
481 known amine-diacid mixtures enable the determination of the ratios of the base to acid in reacted  
482 particles. The relative increase in these ratios for DART-MS compared to those derived by HR-  
483 ToF-MS was used to estimate the probe depth of DART-MS. It is shown that DART-MS probes  
484 mainly the surface layer of the particles, in agreement with other studies on different systems.  
485 Results for  $\alpha$ -cedrene SOA particles show that HMW products are a major component of the  
486 smaller particles, consistent with these products playing an important role in initial particle  
487 formation (Zhao et al., 2016). Vaporization of particles at different temperatures before  
488 introduction into the DART ionization region permits the characterization of isomeric structures  
489 of SOA particles based on their volatility. All of these studies were carried out under dry  
490 conditions. The presence of water vapor would be expected to influence some of the physical  
491 and chemical processes involved in both systems. This remains to be investigated.

492 Some challenges remain in applying DART-MS, for example quantification of individual  
493 compounds. While relative concentrations can be determined by utilizing an internal (Zhou et al.,  
494 2015; Schilling Fahnestock et al., 2015) or external standard (as shown for the amine-diacid  
495 system in our present study), this assumes that DART-MS has the same sensitivity for the  
496 standards and the analytes. This might not hold for SOA particles that consist of a complex  
497 mixture of organic compounds with a wide diversity of functionality and polarity. In addition,  
498 internal standards need to be well-mixed with the sample, which can be difficult if the standard  
499 and analyte recrystallize separately. Furthermore, the standard configuration for DART-MS at  
500 present operates in an open environment so the amount of the analyte actually sampled by the  
501 MS may not be well controlled. As with many other ambient ionization techniques, caution is  
502 warranted with respect to possible oxidation by OH and other reactive species generated in the  
503 source.

504 However, this study in combination with previous work (Nah et al., 2013;Chan et al., 2013;Zhou  
505 et al., 2015;Schilling Fahnstock et al., 2015;Chan et al., 2014;Davies and Wilson, 2015;Zhao et  
506 al., 2016) demonstrates that DART-MS is a very useful complement to ESI-MS and other mass  
507 spectrometric techniques for the analysis of complex atmospherically relevant systems.  
508 Combined with temperature studies, it can provide depth information on spatially heterogeneous  
509 particles and potentially differentiate between isobaric compounds of different volatility.

#### 510 *Acknowledgements*

511 This work was supported by the National Science Foundation (Grants #1207112, #1404233 and  
512 #1443140) and the NSF Major Research Instrumentation (MRI) program (Grants #1337080 and  
513 #0923323). The authors would like to thank Kristine Arquero for assistance with the TMA  
514 permeation tube and measurements of the gas phase TMA concentration.

515 **References**

- 516 Aljawhary, D., Lee, A. K. Y., and Abbatt, J. P. D.: High-resolution chemical ionization mass  
517 spectrometry (ToF-CIMS): application to study SOA composition and processing, *Atmos.*  
518 *Meas. Tech.*, 6, 3211-3224, 2013.
- 519 Angelino, S., Suess, D. T., and Prather, K. A.: Formation of aerosol particles from reactions of  
520 secondary and tertiary alkylamines: characterization by aerosol time-of-flight mass  
521 spectrometry, *Environ. Sci. Technol.*, 35, 3130-3138, 2001.
- 522 Bilde, M., Svenningsson, B., Monster, J., and Rosenorn, T.: Even-odd alternation of evaporation  
523 rates and vapor pressures of C<sub>3</sub>-C<sub>9</sub> dicarboxylic acid aerosols, *Environ. Sci. Technol.*, 37,  
524 1371-1378, 2003.
- 525 Bilde, M., Barsanti, K., Booth, M., Cappa, C. D., Donahue, N. M., Emanuelsson, E. U.,  
526 McFiggans, G., Krieger, U. K., Marcolli, C., Topping, D., Ziemann, P., Barley, M.,  
527 Clegg, S., Dennis-Smith, B., Hallquist, M., Hallquist, A. M., Khlystov, A., Kulmala, M.,  
528 Mogensen, D., Percival, C. J., Pope, F., Reid, J. P., da Silva, M. A. V. R., Rosenoern, T.,  
529 Salo, K., Soonsin, V. P., Yli-Juuti, T., Prisle, N. L., Pagels, J., Rarey, J., Zardini, A. A.,  
530 and Riipinen, I.: Saturation vapor pressures and transition enthalpies of low-volatility  
531 organic molecules of atmospheric relevance: from dicarboxylic acids to complex  
532 mixtures, *Chem. Rev.*, 115, 4115-4156, 2015.
- 533 Bruns, E. A., Greaves, J., and Finlayson-Pitts, B. J.: Measurement of vapor pressures and heats  
534 of sublimation of dicarboxylic acids using atmospheric solids analysis probe mass  
535 spectrometry, *J. Phys. Chem. A.*, 116, 5900-5909, 2012.
- 536 Bzdek, B. R., Lawler, M. J., Horan, A. J., Pennington, M. R., DePalma, J. W., Zhao, J., Smith, J.  
537 N., and Johnston, M. V.: Molecular constraints on particle growth during new particle  
538 formation, *Geophys. Res. Lett.*, 41, 6045-6054, 2014.
- 539 Canagaratna, M. R., Jimenez, J. L., Kroll, J. H., Chen, Q., Kessler, S. H., Massoli, P., Ruiz, L. H.,  
540 Fortner, E., Williams, L. R., Wilson, K. R., Surratt, J. D., Donahue, N. M., Jayne, J. T.,  
541 and Worsnop, D. R.: Elemental ratio measurements of organic compounds using aerosol  
542 mass spectrometry: characterization, improved calibration, and implications, *Atmos.*  
543 *Chem. Phys.*, 15, 253-272, 2015.
- 544 Cappa, C. D., Lovejoy, E. R., and Ravishankara, A. R.: Determination of evaporation rates and  
545 vapor pressures of very low volatility compounds: a study of the C<sub>4</sub>-C<sub>10</sub> and C<sub>12</sub>  
546 dicarboxylic acids, *J. Phys. Chem. A.*, 111, 3099-3109, 2007.
- 547 Chan, M. N., Nah, T., and Wilson, K. R.: Real time *in situ* chemical characterization of sub-  
548 micron organic aerosols using direct analysis in real time mass spectrometry (DART-MS):  
549 the effect of aerosol size and volatility, *Analyst*, 138, 3749-3757, 2013.
- 550 Chan, M. N., Zhang, H. F., Goldstein, A. H., and Wilson, K. R.: Role of water and phase in the  
551 heterogeneous oxidation of solid and aqueous succinic acid aerosol by hydroxyl radicals,  
552 *J. Phys. Chem. C.*, 118, 28978-28992, 2014.
- 553 Chen, H., Venter, A., and Cooks, R. G.: Extractive electrospray ionization for direct analysis of  
554 undiluted urine, milk and other complex mixtures without sample preparation, *Chem.*  
555 *Commun.*, 2042-2044, 2006.
- 556 Chen, H., Sun, Y., Wortmann, A., Gu, H., and Zenobi, R.: Differentiation of maturity and quality  
557 of fruit using noninvasive extractive electrospray ionization quadrupole time-of-flight  
558 mass spectrometry, *Anal. Chem.*, 79, 1447-1455, 2007.
- 559 Chen, H., Varner, M. E., Gerber, R. B., and Finlayson-Pitts, B. J.: Reactions of methanesulfonic  
560 acid with amines and ammonia as a source of new particles in air, *J. Phys. Chem. B.*, 120,

561 1526-1536, 2016.

562 Chingin, K., Gamez, G., Chen, H., Zhu, L., and Zenobi, R.: Rapid classification of perfumes by  
563 extractive electrospray ionization mass spectrometry (EESI-MS), *Rapid Commun. Mass.*  
564 *Sp.*, 22, 2009-2014, 2008.

565 Cody, R. B., Laramée, J. A., and Durst, H. D.: Versatile new ion source for the analysis of  
566 materials in open air under ambient conditions, *Anal. Chem.*, 77, 2297-2302, 2005.

567 Compernelle, S., Ceulemans, K., and Muller, J. F.: EVAPORATION: a new vapour pressure  
568 estimation method for organic molecules including non-additivity and intramolecular  
569 interactions, *Atmos. Chem. Phys.*, 11, 9431-9450, 2011.

570 Davies, J. F., and Wilson, K. R.: Nanoscale interfacial gradients formed by the reactive uptake of  
571 OH radicals onto viscous aerosol surfaces, *Chem. Sci.*, 6, 7020-7027, 2015.

572 Dawson, M. L., Varner, M. E., Perraud, V., Ezell, M. J., Gerber, R. B., and Finlayson-Pitts, B. J.:  
573 Simplified mechanism for new particle formation from methanesulfonic acid, amines,  
574 and water via experiments and *ab initio* calculations, *P. Natl. Acad. Sci. USA.*, 109,  
575 18719-18724, 2012.

576 Dawson, M. L., Perraud, V., Gomez, A., Arquero, K. D., Ezell, M. J., and Finlayson-Pitts, B. J.:  
577 Measurement of gas-phase ammonia and amines in air by collection onto an ion  
578 exchange resin and analysis by ion chromatography, *Atmos. Meas. Tech.*, 7, 2733-2744,  
579 2014.

580 De Haan, D. O., Hawkins, L. N., Kononenko, J. A., Turley, J. J., Corrigan, A. L., Tolbert, M. A.,  
581 and Jimenez, J. L.: Formation of nitrogen-containing oligomers by methylglyoxal and  
582 amines in simulated evaporating cloud droplets, *Environ. Sci. Technol.*, 45, 984-991,  
583 2011.

584 de Semainville, P. G., D'Anna, B., and George, C.: Aqueous phase reactivity of nitrate radicals  
585 ( $\text{NO}_3$ ) toward dicarboxylic acids, *Z. Phys. Chem.*, 224, 1247-1260, 2010.

586 DeCarlo, P. F., Kimmel, J. R., Trimborn, A., Northway, M. J., Jayne, J. T., Aiken, A. C., Gonin,  
587 M., Fuhrer, K., Horvath, T., Docherty, K. S., Worsnop, D. R., and Jimenez, J. L.: Field-  
588 deployable, high-resolution, time-of-flight aerosol mass spectrometer, *Anal. Chem.*, 78,  
589 8281-8289, 2006.

590 Doezema, L., Longin, T., Cody, W., Perraud, V., Dawson, M. L., Ezell, M. J., Greaves, J.,  
591 Johnson, K. R., and Finlayson-Pitts, B. J.: Analysis of secondary organic aerosols in air  
592 using extractive electrospray ionization mass spectrometry (EESI-MS) *RSC Adv.*, 2,  
593 2930-2938, 2012.

594 Duporte, G., Parshintsev, J., Barreira, L. M. F., Hartonen, K., Kulmala, M., and Riekkola, M. L.:  
595 Nitrogen-containing low volatile compounds from pinonaldehyde-dimethylamine  
596 reaction in the atmosphere: A laboratory and field study, *Environ. Sci. Technol.*, 4693–  
597 4700, 2016.

598 Ervens, B., Turpin, B. J., and Weber, R. J.: Secondary organic aerosol formation in cloud droplets  
599 and aqueous particles (aqSOA): a review of laboratory, field and model studies, *Atmos.*  
600 *Chem. Phys.*, 11, 11069-11102, 2011.

601 Farmer, D. K., Cappa, C. D., and Kreidenweis, S. M.: Atmospheric processes and their  
602 controlling influence on cloud condensation nuclei activity, *Chem. Rev.*, 115, 4199-4217,  
603 2015.

604 Finlayson-Pitts, B. J., and Pitts, J. N.: *Chemistry of the Upper and Lower Atmosphere : Theory,*  
605 *Experiments, and Applications*, Academic Press, San Diego, 2000.

606 Gallimore, P. J., and Kalberer, M.: Characterizing an extractive electrospray ionization (EESI)

607 source for the online mass spectrometry analysis of organic aerosols, *Environ. Sci.*  
608 *Technol.*, 47, 7324-7331, 2013.

609 Gao, Y. Q., Hall, W. A., and Johnston, M. V.: Molecular composition of monoterpene secondary  
610 organic aerosol at low mass loading, *Environ. Sci. Technol.*, 44, 7897-7902, 2010.

611 Gard, E., Mayer, J. E., Morrical, B. D., Dienes, T., Ferguson, D. P., and Prather, K. A.: Real-  
612 time analysis of individual atmospheric aerosol particles: design and performance of a  
613 portable ATOFMS, *Anal. Chem.*, 69, 4083-4091, 1997.

614 Ge, X. L., Wexler, A. S., and Clegg, S. L.: Atmospheric amines - part I. A review, *Atmos.*  
615 *Environ.*, 45, 524-546, 2011.

616 George, C., Ammann, M., D'Anna, B., Donaldson, D. J., and Nizkorodov, S. A.: Heterogeneous  
617 Photochemistry in the Atmosphere, *Chem. Rev.*, 115, 4218-4258, 2015.

618 Glasius, M., and Goldstein, A. H.: Recent discoveries and future challenges in atmospheric  
619 organic chemistry, *Environ. Sci. Technol.*, 50, 2754-2764, 2016.

620 Gomez-Hernandez, M., McKeown, M., Secrest, J., Marrero-Ortiz, W., Lavi, A., Rudich, Y.,  
621 Collins, D. R., and Zhang, R. Y.: Hygroscopic characteristics of alkylammonium  
622 carboxylate aerosols, *Environ. Sci. Technol.*, 50, 2292-2300, 2016.

623 Griffiths, P. T., Badger, C. L., Cox, R. A., Folkers, M., Henk, H. H., and Mentel, T. F.: Reactive  
624 uptake of N<sub>2</sub>O<sub>5</sub> by aerosols containing dicarboxylic acids. Effect of particle phase,  
625 composition, and nitrate content, *J. Phys. Chem. A.*, 113, 5082-5090, 2009.

626 Gross, J. H.: Direct analysis in real time-a critical review on DART-MS, *Anal. Bioanal. Chem.*,  
627 406, 63-80, 2014.

628 Hallquist, M., Wenger, J. C., Baltensperger, U., Rudich, Y., Simpson, D., Claeys, M., Dommen, J.,  
629 Donahue, N. M., George, C., Goldstein, A. H., Hamilton, J. F., Herrmann, H., Hoffmann,  
630 T., Iinuma, Y., Jang, M., Jenkin, M. E., Jimenez, J. L., Kiendler-Scharr, A., Maenhaut, W.,  
631 McFiggans, G., Mentel, T. F., Monod, A., Prevot, A. S. H., Seinfeld, J. H., Surratt, J. D.,  
632 Szmigielski, R., and Wildt, J.: The formation, properties and impact of secondary organic  
633 aerosol: current and emerging issues, *Atmos. Chem. Phys.*, 9, 5155-5236, 2009.

634 Herrmann, H., Schaefer, T., Tilgner, A., Styler, S. A., Weller, C., Teich, M., and Otto, T.:  
635 Tropospheric aqueous-phase chemistry: kinetics, mechanisms, and its coupling to a  
636 changing gas phase, *Chem. Rev.*, 115, 4259-4334, 2015.

637 Horan, A. J., Gao, Y. Q., Hall, W. A., and Johnston, M. V.: Online characterization of particles  
638 and gases with an ambient electrospray ionization source, *Anal. Chem.*, 84, 9253-9258,  
639 2012.

640 Huey, L. G.: Measurement of trace atmospheric species by chemical ionization mass  
641 spectrometry: speciation of reactive nitrogen and future directions, *Mass. Spectrom. Rev.*,  
642 26, 166-184, 2007.

643 Jackson, A. U., Werner, S. R., Talaty, N., Song, Y., Campbell, K., Cooks, R. G., and Morgan, J.  
644 A.: Targeted metabolomic analysis of *Escherichia coli* by desorption electrospray  
645 ionization and extractive electrospray ionization mass spectrometry, *Anal. Biochem.*, 375,  
646 272-281, 2008.

647 Jaoui, M., Sexton, K. G., and Kamens, R. M.: Reaction of  $\alpha$ -cedrene with ozone: mechanism,  
648 gas and particulate products distribution, *Atmos. Environ.*, 38, 2709-2725, 2004.

649 Jaoui, M., Kleindienst, T. E., Docherty, K. S., Lewandowski, M., and Offenberg, J. H.:  
650 Secondary organic aerosol formation from the oxidation of a series of sesquiterpenes:  $\alpha$ -  
651 cedrene,  $\beta$ -caryophyllene,  $\alpha$ -humulene and  $\alpha$ -farnesene with O<sub>3</sub>, OH and NO<sub>3</sub> radicals,  
652 *Environ. Chem.*, 10, 178-193, 2013.

653 Jimenez, J. L., Canagaratna, M. R., Donahue, N. M., Prevot, A. S. H., Zhang, Q., Kroll, J. H.,  
654 DeCarlo, P. F., Allan, J. D., Coe, H., Ng, N. L., Aiken, A. C., Docherty, K. S., Ulbrich, I.  
655 M., Grieshop, A. P., Robinson, A. L., Duplissy, J., Smith, J. D., Wilson, K. R., Lanz, V. A.,  
656 Hueglin, C., Sun, Y. L., Tian, J., Laaksonen, A., Raatikainen, T., Rautiainen, J.,  
657 Vaattovaara, P., Ehn, M., Kulmala, M., Tomlinson, J. M., Collins, D. R., Cubison, M. J.,  
658 Dunlea, E. J., Huffman, J. A., Onasch, T. B., Alfarra, M. R., Williams, P. I., Bower, K.,  
659 Kondo, Y., Schneider, J., Drewnick, F., Borrmann, S., Weimer, S., Demerjian, K., Salcedo,  
660 D., Cottrell, L., Griffin, R., Takami, A., Miyoshi, T., Hatakeyama, S., Shimono, A., Sun, J.  
661 Y., Zhang, Y. M., Dzepina, K., Kimmel, J. R., Sueper, D., Jayne, J. T., Herndon, S. C.,  
662 Trimborn, A. M., Williams, L. R., Wood, E. C., Middlebrook, A. M., Kolb, C. E.,  
663 Baltensperger, U., and Worsnop, D. R.: Evolution of organic aerosols in the atmosphere,  
664 *Science*, 326, 1525-1529, 2009.

665 Kawamura, K., and Bikkina, S.: A review of dicarboxylic acids and related compounds in  
666 atmospheric aerosols: molecular distributions, sources and transformation, *Atmos. Res.*,  
667 170, 140-160, 2016.

668 Kolesar, K. R., Li, Z. Y., Wilson, K. R., and Cappa, C. D.: Heating-induced evaporation of nine  
669 different secondary organic aerosol types, *Environ. Sci. Technol.*, 49, 12242-12252, 2015.

670 Kroll, J. H., and Seinfeld, J. H.: Chemistry of secondary organic aerosol: formation and  
671 evolution of low-volatility organics in the atmosphere, *Atmos. Environ.*, 42, 3593-3624,  
672 2008.

673 Kulmala, M., Petaja, T., Ehn, M., Thornton, J., Sipila, M., Worsnop, D. R., and Kerminen, V. M.:  
674 Chemistry of atmospheric nucleation: on the recent advances on precursor  
675 characterization and atmospheric cluster composition in connection with atmospheric  
676 new particle formation, *Annu. Rev. Phys. Chem.*, 65, 21-37, 2014.

677 Laskin, A., Laskin, J., and Nizkorodov, S. A.: Mass spectrometric approaches for chemical  
678 characterisation of atmospheric aerosols: critical review of the most recent advances,  
679 *Environ. Chem.*, 9, 163-189, 2012.

680 Laskin, A., Laskin, J., and Nizkorodov, S. A.: Chemistry of atmospheric brown carbon, *Chem.*  
681 *Rev.*, 115, 4335-4382, 2015.

682 Laskin, J., Laskin, A., and Nizkorodov, S. A.: New mass spectrometry techniques for studying  
683 physical chemistry of atmospheric heterogeneous processes, *Int. Rev. Phys. Chem.*, 32,  
684 128-170, 2013.

685 Lavi, A., Segre, E., Gomez-Hernandez, M., Zhang, R. Y., and Rudich, Y.: Volatility of  
686 atmospherically relevant alkylammonium carboxylate salts, *J. Phys. Chem. A.*, 119, 4336-  
687 4346, 2015.

688 Law, W. S., Wang, R., Hu, B., Berchtold, C., Meier, L., Chen, H. W., and Zenobi, R.: On the  
689 mechanism of extractive electrospray ionization, *Anal. Chem.*, 82, 4494-4500, 2010.

690 Lide, D. R.: *CRC Handbook of Chemistry and Physics*, CRC press, 2004.

691 Liu, Y. C., Ma, Q. X., and He, H.: Heterogeneous uptake of amines by citric acid and humic acid,  
692 *Environ. Sci. Technol.*, 46, 11112-11118, 2012.

693 Lopez-Hilfiker, F. D., Mohr, C., Ehn, M., Rubach, F., Kleist, E., Wildt, J., Mentel, T. F., Lutz, A.,  
694 Hallquist, M., Worsnop, D., and Thornton, J. A.: A novel method for online analysis of  
695 gas and particle composition: description and evaluation of a filter inlet for gases and  
696 AEROSols (FIGAERO), *Atmos. Meas. Tech.*, 7, 983-1001, 2014.

697 Moise, T., Flores, J. M., and Rudich, Y.: Optical properties of secondary organic aerosols and  
698 their changes by chemical processes, *Chem. Rev.*, 115, 4400-4439, 2015.



699 Muller, C., Iinuma, Y., Karstensen, J., van Pinxteren, D., Lehmann, S., Gnauk, T., and Herrmann,  
700 H.: Seasonal variation of aliphatic amines in marine sub-micrometer particles at the Cape  
701 Verde islands, *Atmos. Chem. Phys.*, 9, 9587-9597, 2009a.

702 Muller, L., Reinnig, M. C., Hayen, H., and Hoffmann, T.: Characterization of oligomeric  
703 compounds in secondary organic aerosol using liquid chromatography coupled to  
704 electrospray ionization Fourier transform ion cyclotron resonance mass spectrometry,  
705 *Rapid Commun. Mass. Sp.*, 23, 971-979, 2009b.

706 Murphy, D. M., and Thomson, D. S.: Laser ionization mass-spectroscopy of single aerosol-  
707 particles, *Aerosol Sci. Tech.*, 22, 237-249, 1995.

708 Nah, T., Chan, M., Leone, S. R., and Wilson, K. R.: Real time *in situ* chemical characterization  
709 of submicrometer organic particles using direct analysis in real time-mass spectrometry,  
710 *Anal. Chem.*, 85, 2087-2095, 2013.

711 Ng, N. L., Canagaratna, M. R., Zhang, Q., Jimenez, J. L., Tian, J., Ulbrich, I. M., Kroll, J. H.,  
712 Docherty, K. S., Chhabra, P. S., Bahreini, R., Murphy, S. M., Seinfeld, J. H., Hildebrandt,  
713 L., Donahue, N. M., DeCarlo, P. F., Lanz, V. A., Prevot, A. S. H., Dinar, E., Rudich, Y.,  
714 and Worsnop, D. R.: Organic aerosol components observed in Northern Hemispheric  
715 datasets from aerosol mass spectrometry, *Atmos. Chem. Phys.*, 10, 4625-4641, 2010.

716 Nizkorodov, S. A., Laskin, J., and Laskin, A.: Molecular chemistry of organic aerosols through  
717 the application of high resolution mass spectrometry, *Phys. Chem. Chem. Phys.*, 13,  
718 3612-3629, 2011.

719 Noziere, B., Kaberer, M., Claeys, M., Allan, J., D'Anna, B., Decesari, S., Finessi, E., Glasius, M.,  
720 Grgic, I., Hamilton, J. F., Hoffmann, T., Iinuma, Y., Jaoui, M., Kahnt, A., Kampf, C. J.,  
721 Kourtchev, I., Maenhaut, W., Marsden, N., Saarikoski, S., Schnelle-Kreis, J., Surratt, J. D.,  
722 Szidat, S., Szmigielski, R., and Wisthaler, A.: The molecular identification of organic  
723 compounds in the atmosphere: state of the art and challenges, *Chem. Rev.*, 115, 3919-  
724 3983, 2015.

725 Powelson, M. H., Espelien, B. M., Hawkins, L. N., Galloway, M. M., and De Haan, D. O.:  
726 Brown carbon formation by aqueous-phase carbonyl compound reactions with amines  
727 and ammonium sulfate, *Environ. Sci. Technol.*, 48, 985-993, 2014.

728 Pratt, K. A., and Prather, K. A.: Mass spectrometry of atmospheric aerosols-recent developments  
729 and applications. Part 1: off-line mass spectrometry techniques, *Mass. Spectrom. Rev.*, 31,  
730 1-16, 2012a.

731 Pratt, K. A., and Prather, K. A.: Mass spectrometry of atmospheric aerosols-recent developments  
732 and applications. Part 2: on-line mass spectrometry techniques, *Mass. Spectrom. Rev.*, 31,  
733 17-48, 2012b.

734 Reinnig, M. C., Warnke, J., and Hoffmann, T.: Identification of organic hydroperoxides and  
735 hydroperoxy acids in secondary organic aerosol formed during the ozonolysis of different  
736 monoterpenes and sesquiterpenes by on-line analysis using atmospheric pressure  
737 chemical ionization ion trap mass spectrometry, *Rapid Commun. Mass. Sp.*, 23, 1735-  
738 1741, 2009.

739 Ruehl, C. R., and Wilson, K. R.: Surface organic monolayers control the hygroscopic growth of  
740 submicrometer particles at high relative humidity, *J. Phys. Chem. A.*, 118, 3952-3966,  
741 2014.

742 Schilling Fahnstock, K. A., Yee, L. D., Loza, C. L., Coggon, M. M., Schwantes, R., Zhang, X.,  
743 Dalleska, N. F., and Seinfeld, J. H.: Secondary organic aerosol composition from C<sub>12</sub>  
744 alkanes, *J. Phys. Chem. A.*, 119, 4281-4297, 2015.

745 Smith, J. N., Moore, K. F., McMurry, P. H., and Eisele, F. L.: Atmospheric measurements of sub-  
746 20 nm diameter particle chemical composition by thermal desorption chemical ionization  
747 mass spectrometry, *Aerosol Sci. Tech.*, 38, 100-110, 2004.

748 Sun, Y. R., Chang, W., Ji, H. W., Chen, C. C., Ma, W. H., and Zhao, J. C.: An unexpected  
749 fluctuating reactivity for odd and even carbon numbers in the TiO<sub>2</sub>-based photocatalytic  
750 decarboxylation of C<sub>2</sub>-C<sub>6</sub> dicarboxylic acids, *Chem-Eur. J.*, 20, 1861-1870, 2014.

751 Taketani, F., Kanaya, Y., and Akimoto, H.: Kinetic studies of heterogeneous reaction of HO<sub>2</sub>  
752 radical by dicarboxylic acid particles, *Int. J. Chem. Kinet.*, 45, 560-565, 2013.

753 Thalladi, V. R., Nüsse, M., and Boese, R.: The melting point alternation in  $\alpha,\omega$ -  
754 alkanedicarboxylic acids, *J. Am. Chem. Soc.*, 122, 9227-9236, 2000.

755 Tobias, H. J., Kooiman, P. M., Docherty, K. S., and Ziemann, P. J.: Real-time chemical analysis  
756 of organic aerosols using a thermal desorption particle beam mass spectrometer, *Aerosol*  
757 *Sci. Tech.*, 33, 170-190, 2000.

758 Wang, R., Grohn, A. J., Zhu, L., Dietiker, R., Wegner, K., Gunther, D., and Zenobi, R.: On the  
759 mechanism of extractive electrospray ionization (EESI) in the dual-spray configuration,  
760 *Anal. Bioanal. Chem.*, 402, 2633-2643, 2012.

761 Winkler, P. M., Ortega, J., Karl, T., Cappellin, L., Friedli, H. R., Barsanti, K., McMurry, P. H.,  
762 and Smith, J. N.: Identification of the biogenic compounds responsible for size-dependent  
763 nanoparticle growth, *Geophys. Res. Lett.*, 39, L20815, 2012.

764 Yao, L., Ma, Y., Wang, L., Zheng, J., Khalizov, A., Chen, M. D., Zhou, Y. Y., Qi, L., and Cui, F.  
765 P.: Role of stabilized Criegee intermediate in secondary organic aerosol formation from  
766 the ozonolysis of  $\alpha$ -cedrene, *Atmos. Environ.*, 94, 448-457, 2014.

767 Yatavelli, R. L. N., Lopez-Hilfiker, F., Wargo, J. D., Kimmel, J. R., Cubison, M. J., Bertram, T.  
768 H., Jimenez, J. L., Gonin, M., Worsnop, D. R., and Thornton, J. A.: A chemical ionization  
769 high-resolution time-of-flight mass spectrometer coupled to a micro orifice volatilization  
770 impactor (MOVI-HR-ToF-CIMS) for analysis of gas and particle-phase organic species,  
771 *Aerosol Sci. Tech.*, 46, 1313-1327, 2012.

772 Zelenyuk, A., and Imre, D.: Single particle laser ablation time-of-flight mass spectrometer: an  
773 introduction to SPLAT, *Aerosol Sci. Tech.*, 39, 554-568, 2005.

774 Zhang, H., Xie, C., Liu, Z. K., Gong, J. B., Bao, Y., Zhang, M. J., Hao, H. X., Hou, B. H., and  
775 Yin, Q. X.: Identification and molecular understanding of the odd-even effect of  
776 dicarboxylic acids aqueous solubility, *Ind. Eng. Chem. Res.*, 52, 18458-18465, 2013.

777 Zhang, Q., Jimenez, J. L., Canagaratna, M. R., Allan, J. D., Coe, H., Ulbrich, I., Alfarra, M. R.,  
778 Takami, A., Middlebrook, A. M., Sun, Y. L., Dzepina, K., Dunlea, E., Docherty, K.,  
779 DeCarlo, P. F., Salcedo, D., Onasch, T., Jayne, J. T., Miyoshi, T., Shimojo, A.,  
780 Hatakeyama, S., Takegawa, N., Kondo, Y., Schneider, J., Drewnick, F., Borrmann, S.,  
781 Weimer, S., Demerjian, K., Williams, P., Bower, K., Bahreini, R., Cottrell, L., Griffin, R.  
782 J., Rautiainen, J., Sun, J. Y., Zhang, Y. M., and Worsnop, D. R.: Ubiquity and dominance  
783 of oxygenated species in organic aerosols in anthropogenically-influenced Northern  
784 Hemisphere midlatitudes, *Geophys. Res. Lett.*, 34, L13801, 2007.

785 Zhang, R. Y., Khalizov, A., Wang, L., Hu, M., and Xu, W.: Nucleation and growth of  
786 nanoparticles in the atmosphere, *Chem. Rev.*, 112, 1957-2011, 2012.

787 Zhao, Y., Wingen, L. M., Perraud, V., Greaves, J., and Finlayson-Pitts, B. J.: Role of the reaction  
788 of stabilized Criegee intermediates with peroxy radicals in particle formation and growth  
789 in air, *Phys. Chem. Chem. Phys.*, 17, 12500-12514, 2015.

790 Zhao, Y., Wingen, L. M., Perraud, V., and Finlayson-Pitts, B. J.: Phase, composition, and growth

791 mechanism for secondary organic aerosol from the ozonolysis of  $\alpha$ -cedrene, Atmos.  
792 Chem. Phys., 16, 3245-3264, 2016.  
793 Zhou, S. M., Forbes, M. W., and Abbatt, J. P. D.: Application of direct analysis in real time-mass  
794 spectrometry (DART-MS) to the study of gas-surface heterogeneous reactions: focus on  
795 ozone and PAHs, Anal. Chem., 87, 4733-4740, 2015.  
796 Ziemann, P. J., and Atkinson, R.: Kinetics, products, and mechanisms of secondary organic  
797 aerosol formation, Chem. Soc. Rev., 41, 6582-6605, 2012.  
798  
799

800 **Table 1.**  $R_{B/A}$  values for amine-reacted malonic acid (C<sub>3</sub>), glutaric acid (C<sub>5</sub>), and pimelic acid (C<sub>7</sub>)  
 801 particles derived by DART-MS, HR-ToF-AMS, and calculations.

	$R_{B/A}$ (DART-MS)	$R_{B/A}$ (AMS)	Calculated $R_{B/A}$ from $F_p$ and the particle size distributions <sup>c</sup>
TMA-C <sub>3</sub>	$0.28 \pm 0.07$	$0.14 \pm 0.01$	$0.07 \pm 0.02$
TMA-C <sub>5</sub>	$0.05 \pm 0.02$	$0.03 \pm 0.01$	$0.02 \pm 0.003$
TMA-C <sub>7</sub>	— <sup>a</sup>	$0.01 \pm 0.001$	— <sup>a</sup>
BA-C <sub>3</sub>	$0.40 \pm 0.09$	— <sup>b</sup>	$0.09 \pm 0.03$
BA-C <sub>5</sub>	$0.22 \pm 0.02$	— <sup>b</sup>	$0.07 \pm 0.01$
BA-C <sub>7</sub>	$0.42 \pm 0.06$	— <sup>b</sup>	$0.07 \pm 0.02$

802 <sup>a</sup>No particle-bound amines were detected by DART-MS. <sup>b</sup>Measurements by AMS were not  
 803 performed. <sup>c</sup>See Eq. (3) and (4) in text. Lower limit due to uncertainty in particle density as  
 804 described in text.

805

806

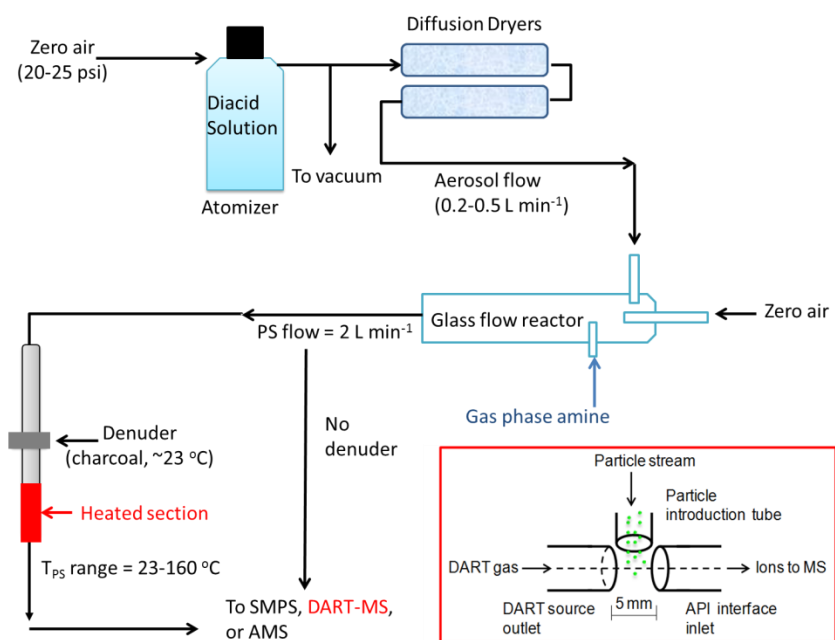
807 **Table 2.** Thickness of the aminium salt shell and DART probe depth for trimethylamine (TMA)-  
 808 reacted malonic acid and glutaric acid.

	<b>R (nm)</b>	<b>r<sub>1</sub> (nm)</b>		<b>r<sub>2</sub> (nm)</b>		<b>L<sub>shell</sub> (nm)</b>		<b>L<sub>DART</sub> (nm)</b>	
		1:1	2:1	1:1	2:1	1:1	2:1	1:1	2:1
Malonic Acid	145	139	140	113	113	5.5	4.5	32	32
Glutaric Acid	135	133	133	106	106	1.7	1.4	28	28

809

810

811

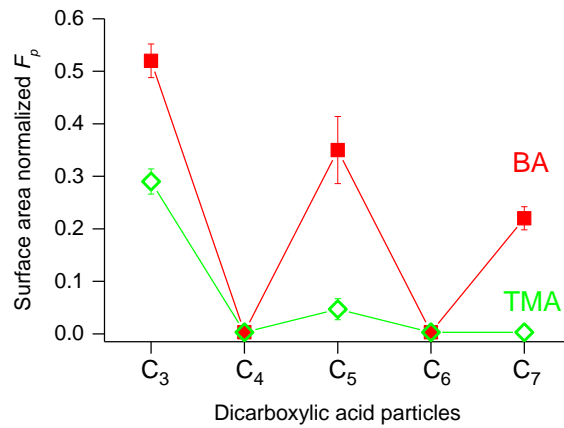


812

813 **Figure 1.** Schematic diagram of the experimental apparatus used for the study of the reaction of  
814 diacid particles with gas phase amines. The inset shows the configuration of DART ion source  
815 interfaced to the MS.

816

817



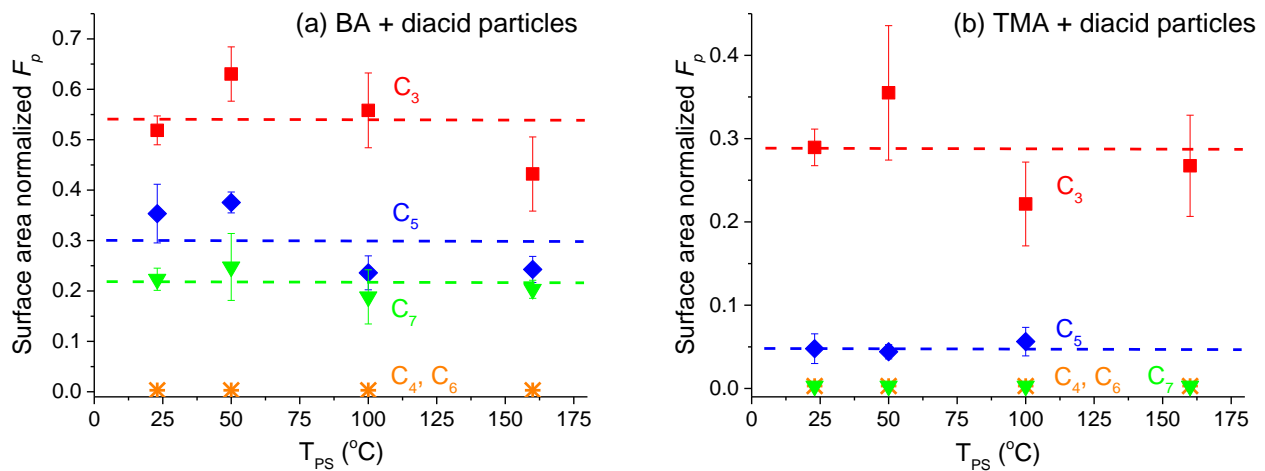
818

819 **Figure 2.** Surface area normalized fraction ( $F_p$ ) of butylamine (solid square) and trimethylamine  
820 (open diamond) in amine-reacted C<sub>3</sub>-C<sub>7</sub> dicarboxylic acid particles measured at  $T_{PS} = 23$  °C.  
821 Error bars are  $\pm 1\sigma$ .

822

823

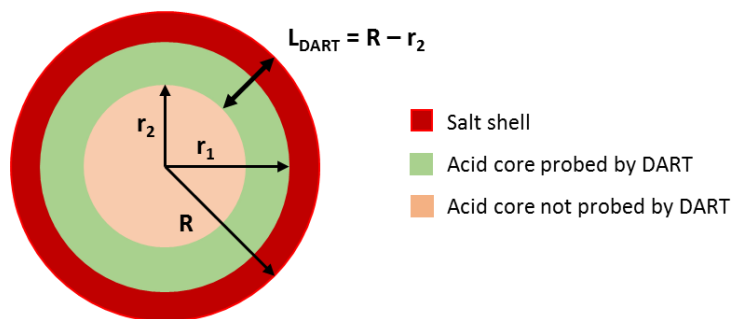
824



825

826 **Figure 3.** Surface area normalized fraction ( $F_p$ ) of (a) butylamine and (b) trimethylamine in  
827 amine-reacted C<sub>3</sub>-C<sub>7</sub> diacid particles measured at different particle stream heating temperatures  
828 ( $T_{PS}$ ). The dashed line represents the average of  $F_p$  values at different  $T_{PS}$ . Error bars are  $\pm 1\sigma$ .

829



830

831 **Figure 4.** Schematic of a typical amine-reacted diacid particle as probed by DART-MS.

832

833

834

835

836

837

838

839

840

841

842

843

844

845

846

847

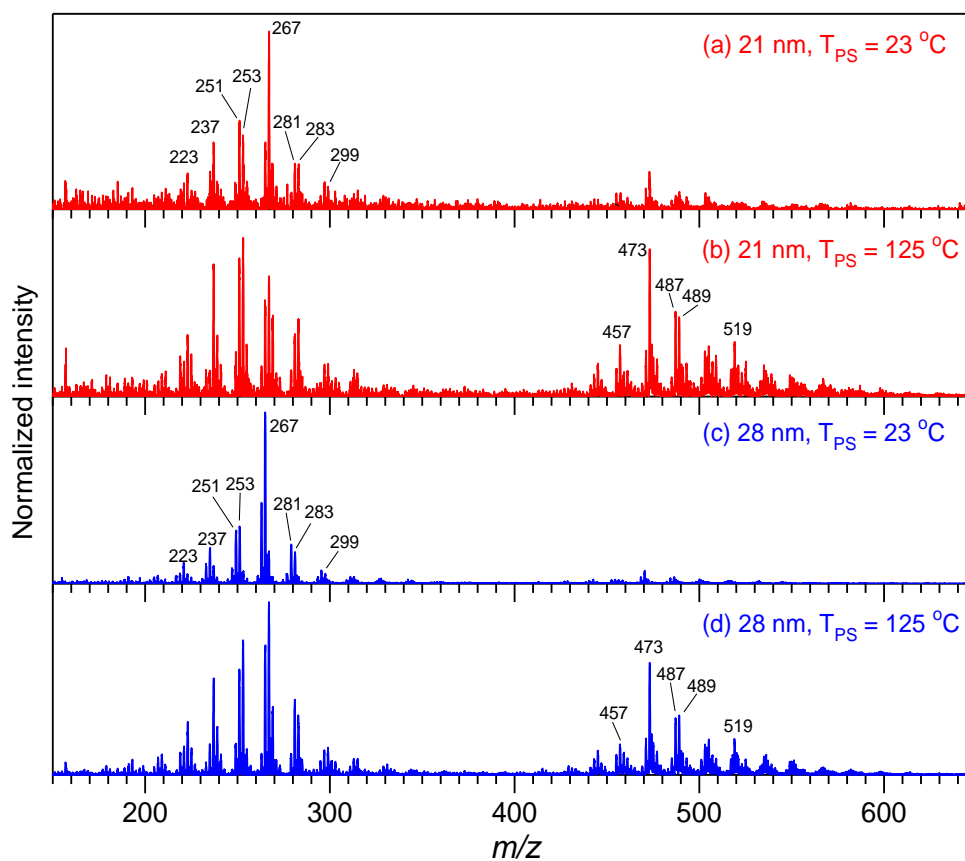
848

849



850

851



852

853 **Figure 5.** DART (-) mass spectra of polydisperse  $\alpha$ -cedrene SOA particles with surface  
854 weighted geometric mean diameters ( $\bar{D}_{g,S}$ ) of 21 nm (a, b) and 28 nm (c, d) at  $T_{PS} = 23$  and 125  
855  $^{\circ}\text{C}$ .  $T_{PS}$  denotes the particle stream temperature before introduction into the DART ionization  
856 region.

857

858  
 859  
 860  
 861  
 862  
 863  
 864  
 865  
 866  
 867  
 868  
 869  
 870  
 871  
 872  
 873  
 874  
 875  
 876  
 877  
 878  
 879  
 880  
 881  
 882

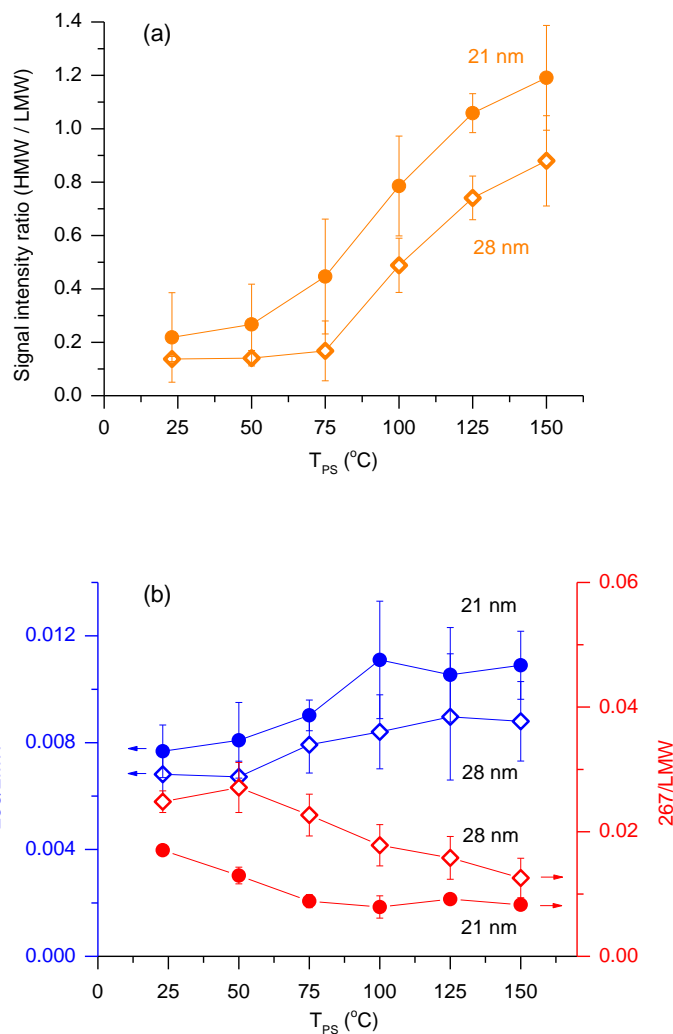


**Figure 6.** The DART-MS signal intensity ratio of (a) high molecular weight (HMW) products ( $m/z$  420-580) to low molecular weight (LMW) products ( $m/z$  200-350) and (b) products at  $m/z$  253 (left y-axis) and  $m/z$  267 (right y-axis) to LMW products ( $m/z$  200-350) for  $\alpha$ -cedrene SOA particles. Data represent particles with  $\bar{D}_{g,S}$  of 21 nm (solid circles) and 28 nm (open diamonds) at different particle stream temperatures ( $T_{PS}$ ). Error bars are  $\pm 1\sigma$ .